

Gamow-Teller properties of the double β -decay partners $^{116}\text{Cd}(\text{Sn})$ and $^{150}\text{Nd}(\text{Sm})$

D. Navas-Nicolás and P. Sarriguren

Instituto de Estructura de la Materia, IEM-CSIC, Serrano 123, E-28006 Madrid, Spain

(Dated: April 23, 2018)

The two Gamow-Teller (GT) branches connecting the double-beta decay partners (^{116}Cd , ^{116}Sn) and (^{150}Nd , ^{150}Sm) with the intermediate nuclei ^{116}In and ^{150}Pm are studied within a microscopic approach based on a deformed proton-neutron quasiparticle random-phase approximation built on a Skyrme selfconsistent mean field with pairing correlations and spin-isospin residual forces. The results are compared with the experimental GT strength distributions extracted from charge-exchange reactions. Combining the two branches, the nuclear matrix elements for the two-neutrino double-beta decay are evaluated and compared to experimental values derived from the measured half-lives.

PACS numbers: 23.40.Hc, 21.60.Jz, 27.60.+j, 27.70.+q

I. INTRODUCTION

Neutrinoless double-beta decay ($0\nu\beta\beta$) is nowadays a topical issue that has attracted a lot of interest from both theoretical and experimental sides [1]. This decay mode is still unobserved and would violate lepton number conservation. Its existence would demonstrate that the neutrino is a massive Majorana particle and would provide a measurement of the absolute mass scale of the neutrino. Obviously, the nuclear matrix element (NME) involved in such a process must be determined accurately to extract a reliable estimate of the neutrino mass. On the other hand, the two-neutrino double-beta decay mode ($2\nu\beta\beta$) is perfectly allowed by the Standard Model. It is a rare second-order weak-interaction process that has been observed experimentally in several nuclei (see Ref. [2] for a review). Thus, to test the reliability of the nuclear structure calculations involved in the $0\nu\beta\beta$ process, one checks first the ability of the nuclear models to reproduce the experimental information available.

Certainly, there are differences between the NMEs involved in both processes, but there are also clear similarities. Among the differences, one should notice that the $2\nu\beta\beta$ -decay NMEs are dominated by Gamow-Teller (GT) transitions connecting the initial and final 0^+ states with all $J^\pi = 1^+$ states in the intermediate nucleus. On the other hand, in the $0\nu\beta\beta$ process the intermediate states run over all J^π values. Another difference with consequences in the evaluation of the NMEs is that in $0\nu\beta\beta$ decay the average virtual neutrino momentum is much larger than the typical scale of nuclear excitations and then closure approximation can be safely used. In the case of $2\nu\beta\beta$ decay the neutrino momenta are comparable with the nuclear excitation energies, preventing the use of closure. Among the similarities, the two processes connect the same initial and final nuclear ground states to be described within a given nuclear model and they share the calculation for the intermediate $J^\pi = 1^+$ states. Therefore, reproducing the $2\nu\beta\beta$ NMEs is a requirement for any nuclear structure model aiming to describe the neutrinoless mode. One can go even further and compare the calculations, not only with the $2\nu\beta\beta$ NMEs extracted from the measured half-lives, which is nothing but a num-

ber, but also with the GT^- (GT^+) strength distribution of the single branch connecting the initial (final) ground state with all the $J^\pi = 1^+$ states in the intermediate nucleus. This comparison provides a more detailed information on which the calculation can be tested. GT strength distributions have been measured in recent years from high resolution charge-exchange reactions (CER), within a large experimental program aimed to explore the GT properties at low excitation energies of double β -decay partners [3–7].

The purpose of this work is to investigate the possibility to describe the rich information available at present on the GT nuclear response within a formalism based on a deformed proton-neutron quasiparticle random-phase approximation (QRPA). This information includes global properties such as the location and strength of the GT resonance, more detailed description in the low-lying excitations, and last but not least, the $2\nu\beta\beta$ -decay NMEs. This study was started for the double β -decay partners with $A = 76, 128, 130$ [8, 9]. Here, we shall focus on the $^{116}\text{Cd} \rightarrow ^{116}\text{Sn}$ and $^{150}\text{Nd} \rightarrow ^{150}\text{Sm}$ decays, motivated by the recent experiments on CER performed for $^{116}\text{Cd}(p, n)^{116}\text{In}$ and $^{116}\text{Sn}(n, p)^{116}\text{In}$ [6], as well as for $^{150}\text{Nd}(^3\text{He}, t)^{150}\text{Pm}$ and $^{150}\text{Sm}(t, ^3\text{He})^{150}\text{Pm}$ [7]. It is also worth mentioning the recent measurement of the electron capture in ^{116}In [10] that can be used as a benchmark for nuclear structure calculations. In addition, the double β decay of ^{150}Nd has received increasing attention in the last years and it is currently considered as one of the best candidates to search for the $0\nu\beta\beta$ decay in the planned experiments SNO+, SuperNEMO, and DCBA. The reason for the interest in ^{150}Nd is that it has a large phase-space factor and therefore a relatively short half-life. It also has a large $Q_{\beta\beta}$ energy that will reduce the background contamination. However, both ^{150}Nd and ^{150}Sm are deformed nuclei that require a deformed formalism to deal with them properly.

The paper is organized as follows: In Sec. II, we present a brief summary of the theoretical approach used to describe the GT strength distributions, as well as the $2\nu\beta\beta$ -decay basic expressions. Section III contains the results obtained from our approach, which are compared to experimental data and other available calculations. Sec-

tion IV contains a summary and the main conclusions.

II. THEORETICAL APPROACH

The description of the deformed QRPA approach used in this work is given elsewhere [11–13]. Here we give only a summary of the method. We start from a self-consistent deformed Hartree-Fock (HF) calculation with effective nucleon-nucleon Skyrme interactions, assuming axial deformation and time reversal symmetry [14]. Most of the results in this work are performed with the Skyrme force SLy4 [15], which is one of the most widely used and successful interactions. In addition, we also present results obtained with other Skyrme forces to investigate their suitability for the description of the spin-isospin properties of nuclei. In particular, besides SLy4, we shall show results from the simpler force Sk3 [16] and from the force SGII [17] that was fitted taking into account nuclear spin-isospin properties.

In our approach, the single-particle wave functions are expanded in terms of the eigenstates of an axially symmetric harmonic oscillator in cylindrical coordinates using twelve major shells. Pairing correlations between like nucleons are included in BCS approximation taking fixed pairing gap parameters for protons and neutrons, which are phenomenologically determined. Besides the selfconsistent HF solution, we also explore the potential energy curves, that is, the HF energy as a function of the quadrupole deformation β , which are obtained from constrained HF+BCS calculations. These results can be seen in Fig. 1 for ^{116}Cd and ^{116}Sn , and in Fig. 2 for ^{150}Nd and ^{150}Sm for the three Skyrme forces considered. We get very soft profiles for ^{116}Cd and ^{116}Sn , whereas for ^{150}Nd and ^{150}Sm we obtain two energy minima, oblate and prolate, but with clear prolate ground states in both cases. We obtain similar results with the three Skyrme forces with the only exception of the force Sk3 in ^{116}Cd , which seems to miss a spherical solution.

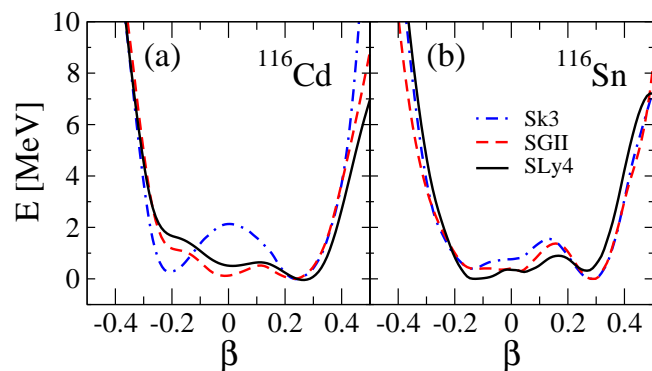


FIG. 1: (Color online) Energy-deformation curves for ^{116}Cd (a) and ^{116}Sn (b) obtained from HF+BCS calculations with various Skyrme forces.

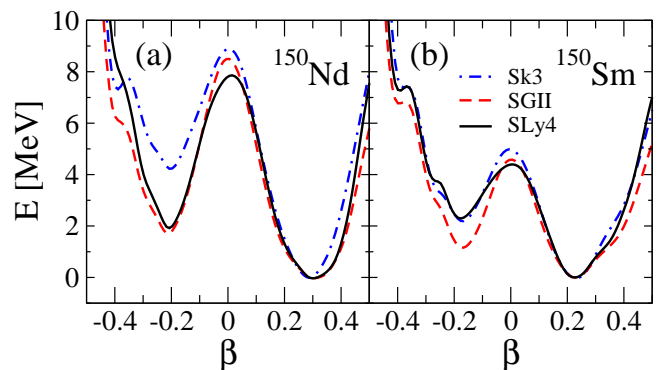


FIG. 2: (Color online) Same as in Fig. 1, but for ^{150}Nd (a) and ^{150}Sm (b).

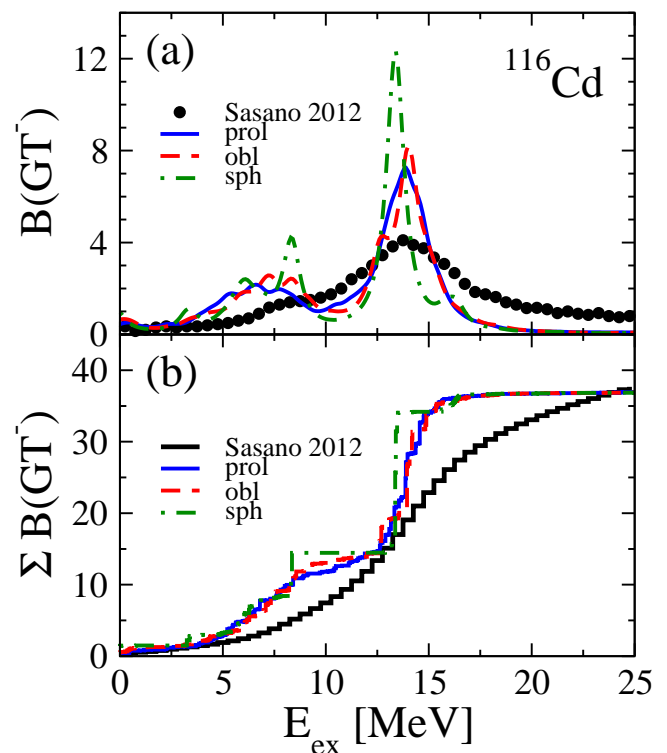


FIG. 3: (Color online) GT strength distributions $B(\text{GT}^-)$ in ^{116}Cd as a function of the excitation energy in the daughter nucleus (a) and accumulated strengths (b). SLy4-QRPA calculations for various deformations are compared to data (Sasano 2012: [6]) from (p, n) reactions.

After the HF+BCS calculation, the QRPA equations are solved on the deformed ground-state basis to get the GT strength distributions and to compute the $2\nu\beta\beta$ -decay NME. To describe GT excitations in QRPA we add to the quasiparticle mean field a separable spin-isospin residual interaction in the particle-hole (ph) and particle-particle (pp) channels. The ph part is responsible for the position and structure of the GT resonance and its cou-

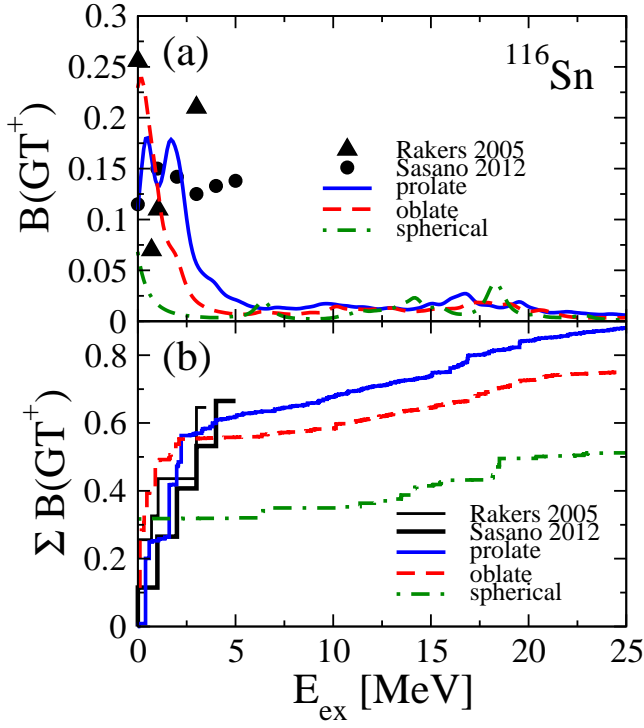


FIG. 4: (Color online) GT strength distributions $B(\text{GT}^+)$ in ^{116}Sn as a function of the excitation energy in the daughter nucleus (a) and accumulated strengths (b). SLy4-QRPA calculations for various deformations are compared to data (Sasano 2012: [6]) from (n,p) reactions, as well as from $(d,^2\text{He})$ (Rakers 2005: [5]).

pling constant χ_{ph}^{GT} is usually taken to reproduce them [11, 18–20]. The pp part consists of a proton-neutron pairing force and it is also introduced as a separable force [12, 19]. The coupling constant κ_{pp}^{GT} is usually fitted to the half-lives phenomenology [20]. In this work we have chosen for the ph and pp coupling constants the law dependence on the mass number A given by $C/A^{0.7}$ in Ref. [20]. However, the different mean fields used, Nilsson [20] versus Skyrme-HF here, make the constants somewhat different. Specifically we use $\chi_{ph}^{GT} = 3.0/A^{0.7}\text{MeV}$ and $\kappa_{pp}^{GT} = 1.8/A^{0.7}\text{MeV}$. Although slightly different values could be used for the different Skyrme forces, we use in this work the same values for them, so that changes among calculations from various forces are caused by the underlying quasiparticle structure provided by the effective Skyrme force. At this point it is worth mentioning the studies on ^{150}Nd and ^{150}Sm carried out in Refs. [21, 22], where deformed QRPA calculations were performed using realistic nucleon-nucleon residual interactions based on the Brueckner G matrix for the CD-Bonn force on top of a phenomenological deformed Woods-Saxon potential. Comparison with the results obtained from schematic separable forces [21] shows that the latter reproduce fairly well the main characteristic of the GT strength distributions profiles and $2\nu\beta\beta$ -decay NMEs.

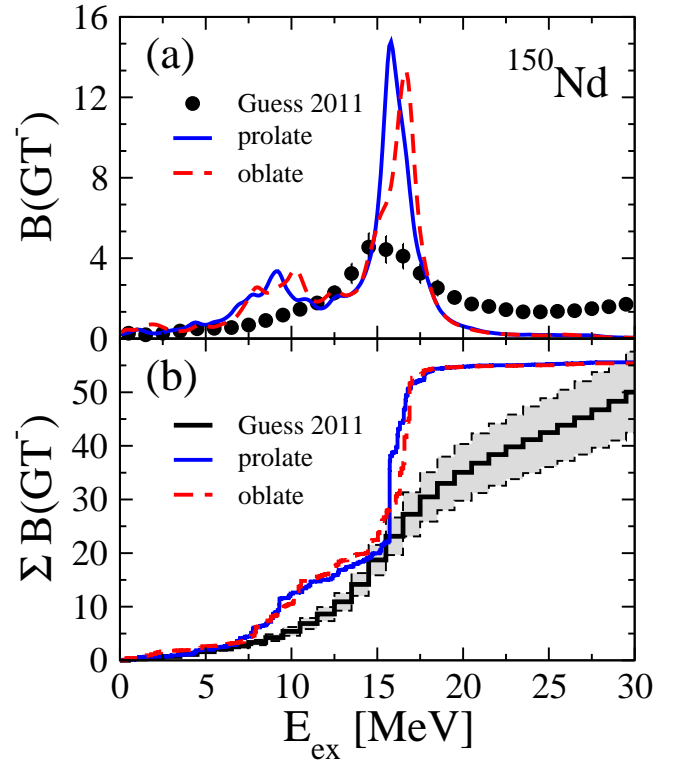


FIG. 5: (Color online) Same as in Fig. 3, but for $B(\text{GT}^-)$ in ^{150}Nd . Data (Guess 2011: [7]) are from $(^3\text{He},t)$ CERs.

The technical details to solve the QRPA equations have been described in Refs. [11, 12, 19]. For each value of the excitation energy, the GT transition amplitudes in the intrinsic frame connecting the ground state $|0\rangle$ to one-phonon states in the daughter nucleus $|\omega_K\rangle$, are found to be

$$\langle \omega_K | \sigma_K t^\pm | 0 \rangle = \mp M_\pm^{\omega_K}, \quad (1)$$

where

$$M_-^{\omega_K} = \sum_{\pi\nu} (v_\nu u_\pi X_{\pi\nu}^{\omega_K} + u_\nu v_\pi Y_{\pi\nu}^{\omega_K}) \langle \nu | \sigma_K | \pi \rangle, \quad (2)$$

$$M_+^{\omega_K} = \sum_{\pi\nu} (u_\nu v_\pi X_{\pi\nu}^{\omega_K} + v_\nu u_\pi Y_{\pi\nu}^{\omega_K}) \langle \nu | \sigma_K | \pi \rangle, \quad (3)$$

in terms of the occupation amplitudes for neutrons and protons $v_{\nu,\pi}$ ($u_{\nu,\pi}^2 = 1 - v_{\nu,\pi}^2$) and the forward and backward amplitudes of the QRPA phonon operator, $X_{\pi\nu}^{\omega_K}$ and $Y_{\pi\nu}^{\omega_K}$, respectively. Once the intrinsic amplitudes in Eq. (1) are calculated, the GT strength $B(\text{GT})$ in the laboratory frame for a transition $I_i K_i(0^+0) \rightarrow I_f K_f(1^+K)$ can be obtained as

$$B_\omega(\text{GT}^\pm) = \sum_{\omega_K} \left[\langle \omega_{K=0} | \sigma_0 t^\pm | 0 \rangle^2 \delta(\omega_{K=0} - \omega) + 2 \langle \omega_{K=1} | \sigma_1 t^\pm | 0 \rangle^2 \delta(\omega_{K=1} - \omega) \right]. \quad (4)$$

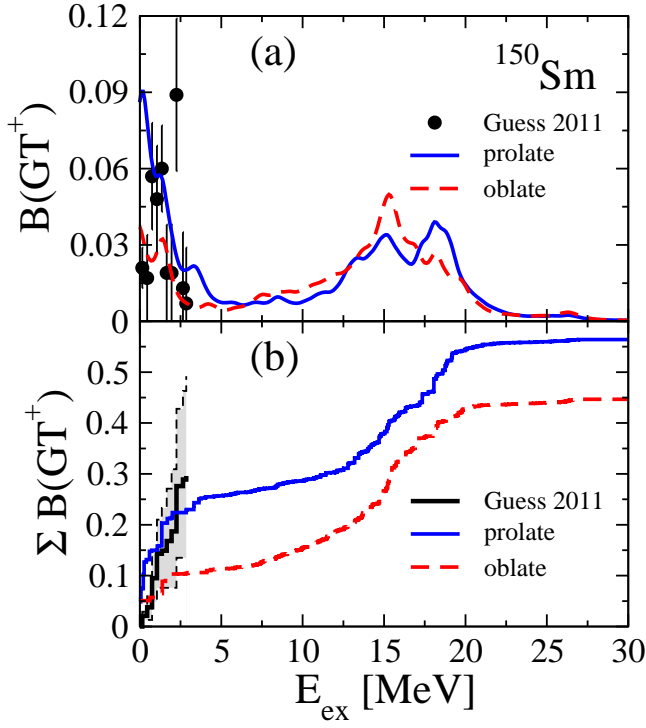


FIG. 6: (Color online) Same as in Fig. 4, but for $B(GT^+)$ in ^{150}Sm . Data (Guess 2011: [7]) are from $(t, {}^3\text{He})$ CERs.

To obtain this expression we have used the initial and final states in the laboratory frame expressed in terms of the intrinsic states using the Bohr and Mottelson factorization. Finally, a quenching factor $q = g_A/g_{A,\text{bare}} = 0.79$ is included in the calculations to take into account in an effective way all the correlations that are not properly considered in the present approach. We shall discuss later in Subsec. III B various attempts aiming to fit simultaneously single- β and double- β decay observables by adjusting the quenching factor.

Concerning the $2\nu\beta\beta$ -decay NMEs, the basic expressions for this process, within the deformed QRPA formalism used in this work, can be found in Refs. [13, 23, 24]. Deformation effects on the $2\nu\beta\beta$ NMEs have been also studied within the Projected Hartree-Fock-Bogoliubov model [25]. Attempts to describe deformation effects on the $0\nu\beta\beta$ decay within QRPA models can also be found in Refs. [26, 27]. The half-life of the $2\nu\beta\beta$ decay can be written as

$$\left[T_{1/2}^{2\nu\beta\beta} (0_{\text{gs}}^+ \rightarrow 0_{\text{gs}}^+) \right]^{-1} = (g_A)^4 G^{2\nu\beta\beta} \left| M_{GT}^{2\nu\beta\beta} \right|^2, \quad (5)$$

in terms of the phase-space integral $G^{2\nu\beta\beta}$ and the nuclear matrix element $M_{GT}^{2\nu\beta\beta}$ that contains all the information of the nuclear structure involved in the process,

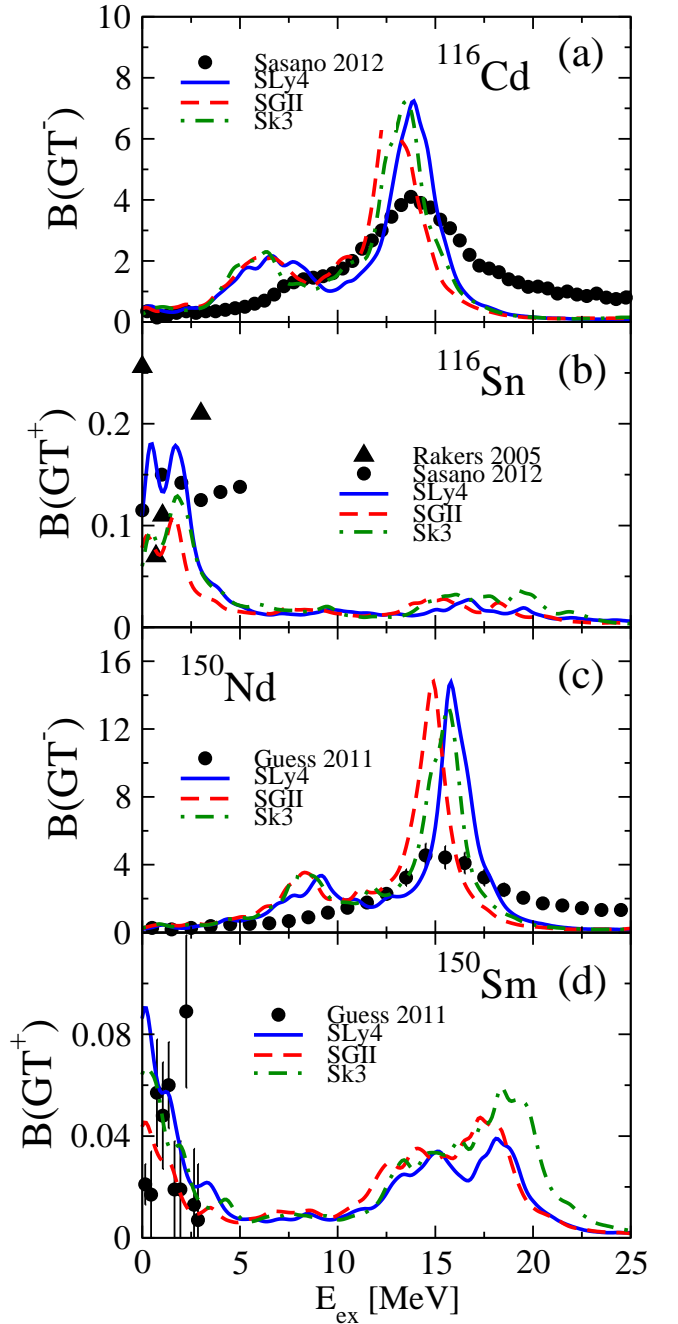


FIG. 7: (Color online) GT strength distributions in ^{116}Cd (a), ^{116}Sn (b), ^{150}Nd (c), and ^{150}Sm (d). The results correspond to the prolate shapes with the Skyrme forces SLy4, SGII, and Sk3. Data are as in the previous figures.

$$M_{GT}^{2\nu\beta\beta} = \sum_{K=0,\pm 1} \sum_{m_i, m_f} (-1)^K \frac{\langle \omega_{K, m_f} | \omega_{K, m_i} \rangle}{D} \times \langle 0_f | \sigma_{-K} t^- | \omega_{K, m_f} \rangle \langle \omega_{K, m_i} | \sigma_{K} t^- | 0_i \rangle. \quad (6)$$

In this equation $|\omega_{K, m_i}\rangle (|\omega_{K, m_f}\rangle)$ are the QRPA intermediate 1^+ states reached from the initial (final) nucleus.

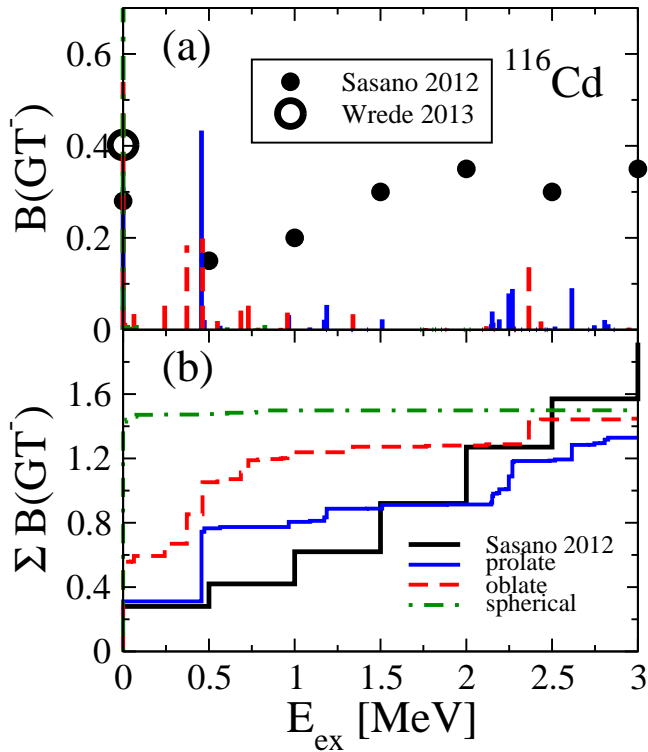


FIG. 8: (Color online) Same as in Fig. 3, but in the low energy range. Also shown is the GT strength extracted from electron capture of ^{116}In (Wrede 2013: [10]).

The indices m_i, m_f label the 1^+ states of the intermediate nucleus. The GT matrix elements are those in Eq. (1). The overlaps are needed to take into account the non-orthogonality of the intermediate states reached from different initial $|0_i\rangle$ and final $|0_f\rangle$ ground states. Their expressions can be found in Ref. [23]. The energy denominator D involves the energy of the emitted leptons, which is given on average by $\frac{1}{2}Q_{\beta\beta} + m_e$, as well as the excitation energies of the intermediate nucleus. In terms of the QRPA excitation energies the denominator can be written as

$$D_1 = \frac{1}{2}(\omega_K^{m_f} + \omega_K^{m_i}), \quad (7)$$

where $\omega_K^{m_i}(\omega_K^{m_f})$ is the QRPA excitation energy relative to the initial (final) nucleus. It turns out that the NMEs are quite sensitive to the values of the denominator, especially for low-lying states when the denominator reaches smaller values. Thus, it is a common practice to use some experimental normalization of this denominator trying to improve the accuracy of the NMEs. In this work we shall also consider the denominator D_2 , which is corrected with the experimental energy $\bar{\omega}_{1^+}$ of the first 1^+ state in the intermediate nucleus relative to the mean ground-state energy of the initial and final nuclei, in such a way that the first calculated 1^+ state appears at the exact experimental energy,

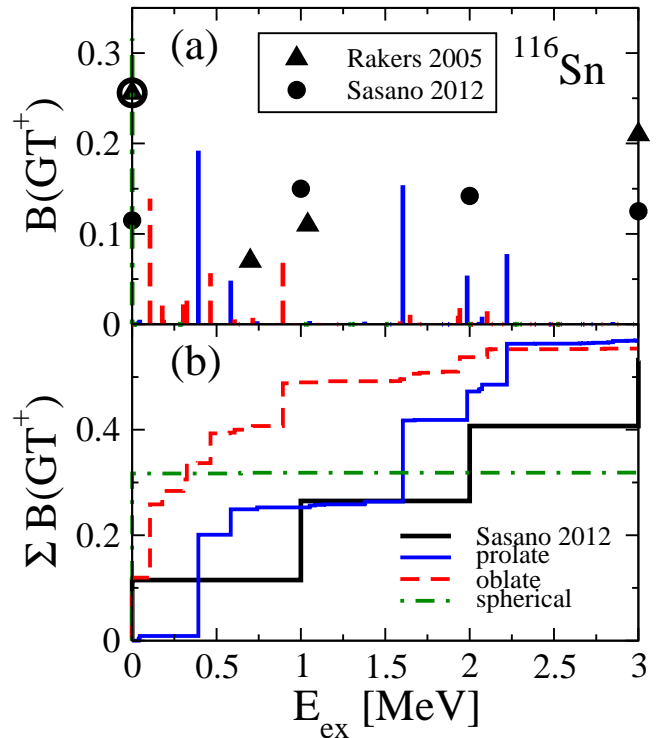


FIG. 9: (Color online) Same as in Fig. 4, but in the low energy range. Also shown (open circle) is the GT strength extracted from β^- decay of ^{116}In to which the data from [5] are normalized.

$$D_2 = \frac{1}{2} \left[\omega_K^{m_f} + \omega_K^{m_i} - (\omega_K^{1_f} + \omega_K^{1_i}) \right] + \bar{\omega}_{1^+}. \quad (8)$$

The running $2\nu\beta\beta$ sums calculated later, will be shown for the two choices of the denominator D_1 and D_2 . In the case of the $A = 116$ isobars, the ground state in the intermediate nucleus ^{116}In is a 1^+ state. Then, the energy $\bar{\omega}_{1^+}$ is given by

$$\bar{\omega}_{1^+} = \frac{1}{2}(Q_{EC} + Q_{\beta^-})_{\text{exp}}, \quad (9)$$

written in terms of the experimental energies $Q_{EC} = 0.463$ MeV and $Q_{\beta^-} = 3.276$ MeV of the decays of ^{116}In into ^{116}Cd and ^{116}Sn , respectively. In the case of $A = 150$, although the ground state in ^{150}Pm is not a 1^+ state, the first 1^+ state excited in CERs appears at a very low excitation energy, $E=0.11$ MeV [7]. Hence, we also determine $\bar{\omega}_{1^+}$ from the experimental values of $Q_{EC} = 0.083$ MeV and $Q_{\beta^-} = 3.456$ MeV for the decays of ^{150}Pm into ^{150}Nd and ^{150}Sm , respectively.

The various measurements reported for the $2\nu\beta\beta$ -decay half-lives ($T_{1/2}^{2\nu\beta\beta}$) have been analyzed in Ref. [2], where recommended values of $T_{1/2}^{2\nu\beta\beta}(^{116}\text{Cd})=(2.8\pm 0.2)\times 10^{19}$ yr and $T_{1/2}^{2\nu\beta\beta}(^{150}\text{Nd})=(8.2\pm 0.9)\times 10^{18}$ yr were

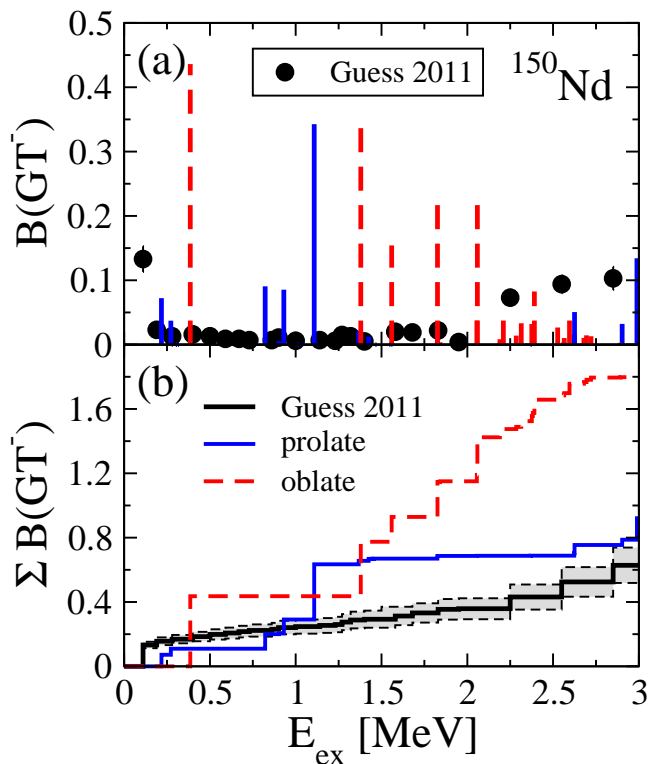


FIG. 10: (Color online) Same as in Fig. 5, but in the low energy range.

adopted. Using the phase-space factors from the recent evaluation [28] that involves exact Dirac wave functions with finite nuclear size and electron screening, $G^{2\nu\beta\beta}({}^{116}\text{Cd})=2.76410^{-18} \text{ yr}^{-1}$, and $G^{2\nu\beta\beta}({}^{150}\text{Nd})=3.64310^{-17} \text{ yr}^{-1}$, one gets the experimental nuclear matrix elements $M_{GT}^{2\nu\beta\beta}({}^{116}\text{Cd})=0.138 \text{ MeV}^{-1}$ (0.223 MeV^{-1}) when the bare $g_{A,\text{bare}} = 1.273$ (quenched factor $g_A = 1$) is used, and $M_{GT}^{2\nu\beta\beta}({}^{150}\text{Nd})=0.070 \text{ MeV}^{-1}$ (0.114 MeV^{-1}) when $g_{A,\text{bare}} = 1.273$ ($g_A = 1$) is used.

III. RESULTS

A. Gamow-Teller strength distributions

Next we discuss the results obtained for the energy distributions of the GT strength. In the upper panels (a) of Figs. 3 and 4 we can see the GT strength distributions for ^{116}Cd ($B(\text{GT}^-)$) and ^{116}Sn ($B(\text{GT}^+)$), respectively. The lower panels (b) show the respective accumulated GT strengths. We compare our QRPA results from SLy4 obtained for prolate, oblate, and spherical shapes in the initial (^{116}Cd) and final (^{116}Sn) nuclei with the experimental strengths extracted from $^{116}\text{Sn}(d,^2\text{He})^{116}\text{In}$ CERS [5] and from $^{116}\text{Cd}(p,n)^{116}\text{In}$ and $^{116}\text{Sn}(n,p)^{116}\text{In}$ CERS [6]. One should notice that the measured strength extracted from the cross sections contains two types of

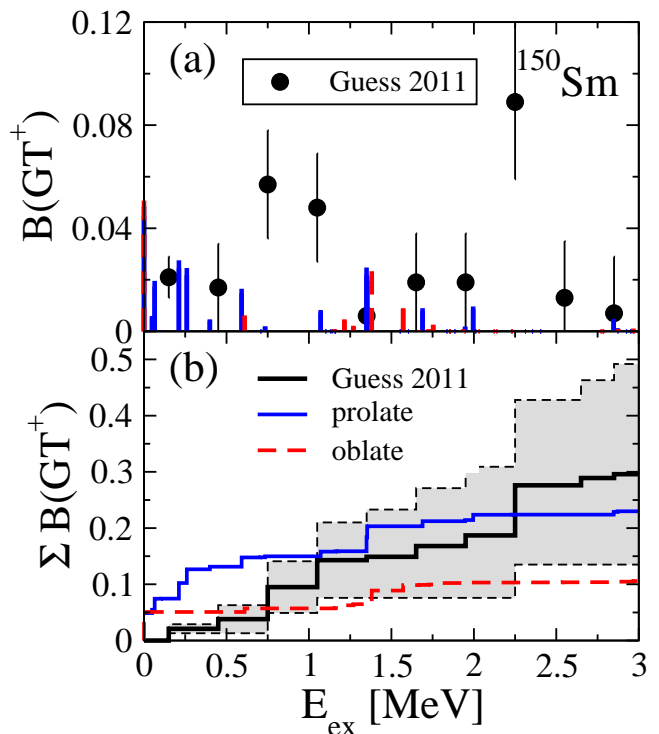


FIG. 11: (Color online) Same as in Fig. 6, but in the low energy range.

contributions, namely GT (σt^\pm operator) and isovector spin monopole (IVSM) ($r^2 \sigma t^\pm$ operator). Both are associated to $\Delta L = 0$ and $\Delta S = 1$ transitions and therefore, they have similar angular distributions that cannot be disentangled in the experiment. Thus, the measured strength corresponds actually to $B(\text{GT}+\text{IVSM})$. Different theoretical calculations evaluating the contributions from both GT and IVSM modes are available in the literature [6, 29–31]. In Ref. [29] a self-consistent Skyrme Hartree-Fock plus Tamm-Dancoff approximation was used to separate the GT from the IVSM strength. Well separated centroids of both resonances were found, with the IVSM resonance at much higher energy, as it corresponds to a $2\hbar\omega$ mode. Subsequent calculations including $A = 116$ isobars were performed in Refs. [30, 31] with different degrees of complexity, from a schematic single-particle model space up to realistic calculations within a QRPA approach in a Woods-Saxon basis and two-body interactions constructed with the Bonn-A potential. In Ref. [6] the contribution from the IVSM component was also evaluated by employing a microscopic method based on QRPA with residual interactions obtained from the Brueckner G-matrix for CD-Bonn nucleon-nucleon force. In general, the conclusions of those theoretical calculations converge in an overall picture. In the (p, n) direction the strength distribution is dominated by the GT component up to about 20 MeV, although non-negligible contributions from IVSM com-

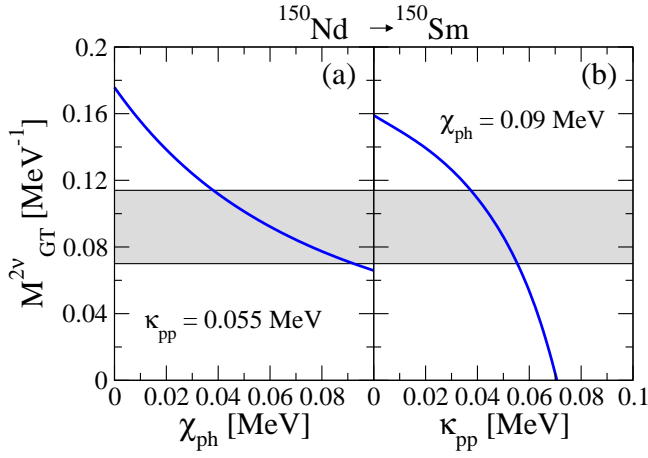


FIG. 12: (Color online) Nuclear matrix element for the $2\nu\beta\beta$ decay of ^{150}Nd as a function of the coupling strengths χ_{ph}^{GT} (a) and κ_{pp}^{GT} (b) for prolate shapes in both ^{150}Nd and ^{150}Sm . The shaded area indicates the experimental range extracted from the measured half-life using bare $g_A = 1.273$ (lower line) and quenched $g_A = 1$ (upper line) factors.

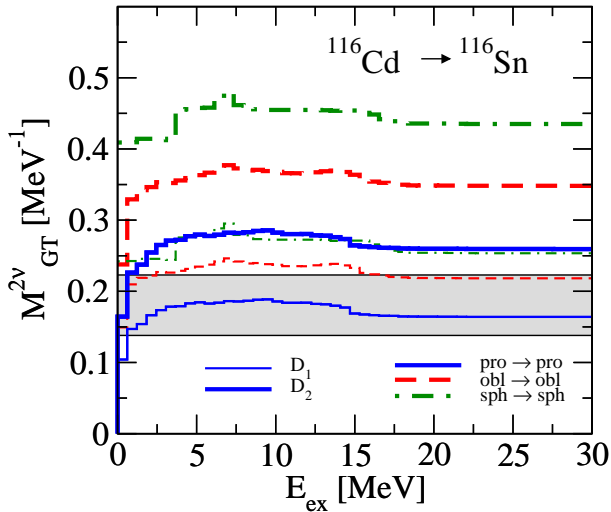


FIG. 13: (Color online) Running sums of the $2\nu\beta\beta$ NME in ^{116}Cd as a function of the intermediate excitation energy in ^{116}In for various calculations using different quadrupole deformations for parent and daughter nuclei. Thin lines correspond to calculations with the energy denominator D_1 (7) while thick lines correspond to D_2 (8).

ponents are found between 10 and 20 MeV, overlapping with the GT strength of the GT giant resonance. Above this energy, there is no significant amount of GT strength in the calculations. The interference effects are constructive below 20 MeV and destructive above this energy, but they are not very important. In the (n,p) direction the GT strength is expected to be strongly Pauli blocked in nuclei with more neutrons than protons and therefore, the measured strength is mostly due to the IVSM

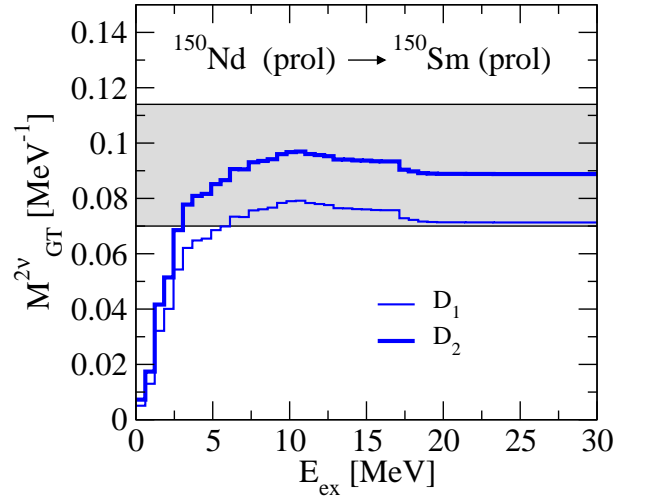


FIG. 14: (Color online) Same as in Fig. 13, but for the double- β decay of ^{150}Nd .

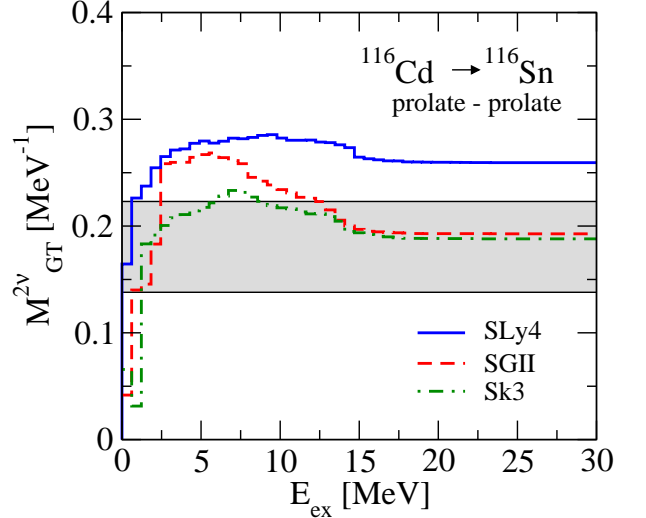


FIG. 15: (Color online) Running sums of the $2\nu\beta\beta$ NME in ^{116}Cd as a function of the intermediate excitation energy in ^{116}In for the decay between prolate shapes. The results are obtained with the energy denominator D_2 for three different Skyrme forces.

resonance over the whole excitation-energy range. Nevertheless, the strength found in low-lying isolated peaks is associated with GT transitions because the continuous tail of the IVSM resonance is very small at these energies and is not expected to exhibit any peak. In summary, the measured strength in the (p,n) direction can be safely assigned to be GT in the low energy range below 10 MeV and with some caution between 10 and 20 MeV. Beyond 20 MeV the strength would be practically due to IVSM. On the other hand the measured strength in the (n,p) direction would be due to IVSM

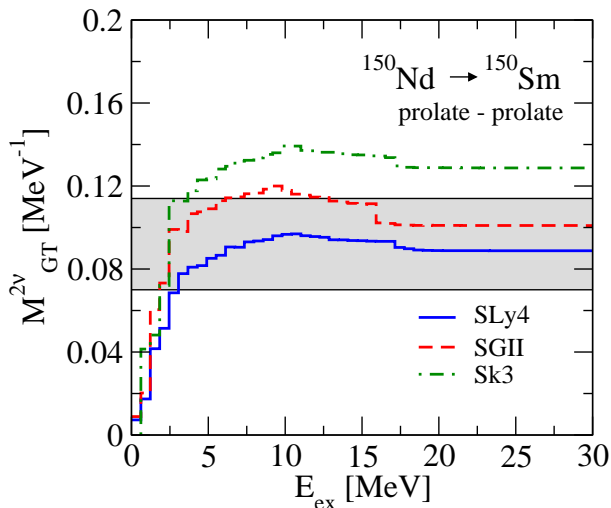


FIG. 16: (Color online) Same as in Fig. 15, but for the decay of ^{150}Nd .

transitions, except in the low-lying excitation energy below several MeV, where the isolated peaks observed can be attributed to GT strength. This is the reason why we plot experimental data in Fig. 4 only up to 5 MeV.

Calculations for the GT strength distributions in both directions $B(\text{GT}^\pm)$ for the $A = 116$ isobars are also available from spherical QRPA calculations within a Woods-Saxon basis and two-body Bonn-A realistic interactions [32]. The results from this reference are quite similar to those in Figs. 3 and 4, although a direct comparison is not easy as they are obtained for particular values of both the strength of the pp residual interaction and the effective g_A value. The $B(\text{GT}^-)$ strength distribution calculated in Ref. [32] is characterized by some marginal strength up to an excitation energy of 5 MeV, then a small bump develops between 7 and 10 MeV, and finally the GT resonance appears between 11 and 15 MeV. Both the energy location of the bumps and the strength contained agree with the features observed in Fig. 3. Similarly, the $B(\text{GT}^+)$ distributions in Ref. [32] and in the corresponding Fig. 4 in this work, contain a similar amount of strength concentrated in the very low-lying excitation energy.

Figs. 5 and 6 show the results for ^{150}Nd and ^{150}Sm , respectively. We compare the QRPA results from SLy4 for prolate and oblate shapes with the data from $(^3\text{He}, t)$ on ^{150}Nd and from $(t, ^3\text{He})$ on ^{150}Sm in Ref. [7]. In general terms, we reproduce fairly well the global properties of the GT strength distributions, including the location of the GT resonance and the total strength measured, although the experimental GT resonances appear more fragmented than the calculated ones. Similar comments to the previous case $A = 116$ relative to the contributions from GT and IVSM components apply now to the case $A = 150$. Microscopic QRPA calculations with residual interactions obtained from the CD-Bonn potential were

performed in Ref. [7] to estimate the GT and IVSM components of the strength $B(\text{GT}+\text{IVSM})$ measured. From this analysis it was also concluded that the strength $B(\text{GT}^-+\text{IVSM}^-)$ below 20 MeV correspond to a large extent to GT strength, whereas the measured strength $B(\text{GT}^++\text{IVSM}^+)$ below 3 MeV could be assigned to the GT component.

In Fig. 7 we show the results for the GT^\pm strength distributions obtained with three different Skyrme forces to see the sensitivity of these distributions to the nucleon-nucleon effective interaction used in the calculations. We can see that the profiles obtained with the three forces are quite similar. The GT^- resonances appear at close energies and contain about the same strength for the three interactions. The GT^+ strength is very small compared to the GT^- and is concentrated for the three forces in the excitation energy region below 5 MeV, with a bump in ^{150}Sm centered at about 15 MeV.

Figures 8, 9, 10, and 11 show in more detail the GT strength distributions with SLy4 in the low excitation-energy range. In the case of ^{116}Cd (Fig. 8) we have included, in addition, the experimental GT strength measured by ground-state to ground-state electron capture on ^{116}In [10]. This value agrees well with the strength obtained with the prolate shape and to a less extent with the oblate one, but it is too low compared to the spherical calculation. Similarly, in the case of ^{116}Sn (Fig. 9) we show with an open circle the experimental GT strength measured by the ground-state to ground-state β^- decay ($^{116}\text{In} \rightarrow ^{116}\text{Sn}$). One should notice that the $B(\text{GT})$ strength from Ref. [5] is calibrated to this value. Although a detailed spectroscopy is beyond the capabilities of our model and the isolated transitions are not well reproduced by our calculations, the overall agreement with the total strength contained in this reduced energy interval, as well as with the profiles of the accumulated strength distributions is reasonable, especially for the prolate shapes in both $A = 116$ partners in Figs. 8 and 9, as well as with the prolate profiles in the $A = 150$ partners displayed in Figs. 10 and 11.

B. Double-beta decay

It is well known that the $2\nu\beta\beta$ NMEs are very sensitive to the residual interactions, as well as to differences in deformation between initial and final nuclei [13, 23]. To illustrate the dependence of the NMEs to the residual forces, we show in Fig. 12 the SLy4-QRPA results with prolate shapes for the $^{150}\text{Nd} \rightarrow ^{150}\text{Sm}$ for various strengths of the coupling constants χ_{ph}^{GT} and κ_{pp}^{GT} . The shaded region corresponds to the experimental NMEs extracted from the measured $2\nu\beta\beta$ half-lives, using bare ($g_A = 1.273$) or quenched ($g_A = 1$) values. We can see that the experimental NMEs contained in the shaded region are reproduced in windows of the parameters that include the values used in this work ($\chi_{ph}^{GT} = 0.09$ MeV and $\kappa_{pp}^{GT} = 0.055$ MeV in ^{150}Nd).

In the next figures we show the running sums for the $2\nu\beta\beta$ NMEs. These are the partial contributions to the NMEs of all the 1^+ states in the intermediate nucleus up to a given energy. We see in Fig. 13 the running sums for the $2\nu\beta\beta$ decay in ^{116}Cd for three combinations of the initial and final nuclear shapes. The NMEs of crossing deformations produce much lower values than the experimental window and are not shown. Similarly, we show in Fig. 14 the running sums for the $^{150}\text{Nd} \rightarrow ^{150}\text{Sm}$ decay using prolate shapes for both nuclei. Results obtained with the energy denominator D_1 (7) are displayed with thin lines, whereas results obtained with D_2 (8) are shown with thick lines. We can see that D_2 denominators produce larger NMEs than D_1 . The main difference is originated at low excitation energies, where the relative effect of using shifted energies is enhanced. The effect at larger energies is negligible and we get a constant difference between D_1 and D_2 , which is the difference accumulated in the first few MeVs. We also observe negative contributions coming from the region of the GT resonances at about 15 MeV. This feature was studied in Ref. [22] and was related to the strength of the pp residual interaction. The small contribution to the $2\nu\beta\beta$ NMEs from the region of the GT resonance is due to the joint effects of large energy denominators in Eq. (6) and the mismatch between the branches of the GT^- and GT^+ excitations in the energy region of the GT resonance.

In Figs. 15 and 16 we have the $2\nu\beta\beta$ NMEs calculated with the denominator D_2 for three Skyrme forces in ^{116}Cd and ^{150}Nd , respectively. The results correspond to the prolate shapes in both initial and final nuclei. The sensitivity of the NMEs to the Skyrme interaction is manifest in the figures, but it is not as significant as the sensitivity found to other aspects such as the residual interactions, the deformation, or even the energy denominators.

Another issue worth to comment is the treatment of the quenching factor of the axial-vector coupling constant g_A . The physical reasons for this quenching have been studied elsewhere [33–35] and are related to the role of non-nucleonic degrees of freedom, absent in the usual theoretical models, and to the limitations of model space, many-nucleon configurations, and deep correlations missing in these calculations. The implications of this quenching on the description of single- β and double- β decay observables have been considered recently in several works [32, 36–39]. In those works both the effective value of g_A and the coupling strength of the residual interaction in the particle-particle channel are considered free parameters of the calculation. The striking result found is that very strong quenching values are needed to reproduce simultaneously the observations corresponding to the $2\nu\beta\beta$ half-lives and to the single- β decay branches, namely $\log ft(EC)$ values for the ground state to ground state decay of the intermediate nucleus into the initial one, and the $\log ft(\beta^-)$ values for the ground state to ground state decay of the intermediate nucleus into the final one. Different procedures for adjusting those parameters have been explained in Refs.

[32, 36–39]. The most recent analysis performed in Ref. [32] within a QRPA formalism comes to the conclusion that considerable quenching is needed, with an average value $\langle g_A \rangle \approx 0.6 \pm 0.2$ ($q = 0.47 \pm 0.16$). The need of a strong quenching is also required in other theoretical approaches, such as different QRPA calculations ($q = 0.6 - 0.7$) [37], IBM-2 models [38], where the quenching obtained is $g_A = 0.41$ ($q = 0.32$) for ^{116}Cd and $g_A = 0.35$ ($q = 0.28$) for ^{150}Nd , or shell-model calculations that found quenching factors in the interval $q = 0.45 - 0.74$ [39] for double- β emitters from ^{48}Ca up to ^{150}Nd .

One should note that the QRPA calculations leading to the strong quenching that fits the $2\nu\beta\beta$ NMEs have been performed within a spherical formalism neglecting possible effects from deformation degrees of freedom. Because the main effect of deformation is a reduction of the NMEs, deformed QRPA calculations shall demand less quenching to fit the experiment. Although the goal of this paper is not to extract consequences on the quenching needed to fit the experiment, it will be very interesting to explore in the future the implications of deformation. This study will be part of a more ambitious project aiming to extract an effective g_A value that fits the decay observables taking into account the uncertainties related to the theoretical description and including all possible $2\nu\beta\beta$ -decay candidates.

IV. SUMMARY AND CONCLUSIONS

In summary, using a theoretical approach based on a deformed HF+BCS+QRPA calculations with effective Skyrme interactions, pairing correlations, and spin-isospin residual separable forces in the ph and pp channels, we have studied simultaneously the GT strength distributions of the double- β decay partners (^{116}Cd , ^{116}Sn) and (^{150}Nd , ^{150}Sm), reaching the intermediate nuclei ^{116}In and ^{150}Pm , respectively, as well as their $2\nu\beta\beta$ NMEs. Our results for the energy distributions of the GT strength have been compared to recent data from charge-exchange reactions, whereas the calculated $2\nu\beta\beta$ NMEs have been compared with the experimental values extracted from the measured half-lives for these processes.

We have discussed the sensitivity of our results to the various ingredients in the theoretical formalism. Namely, to the Skyrme force, to the residual interactions, to deformation, to effective g_A values, and to the treatment of the energy denominators of the NMEs. We found different sensitivities to them that have been analyzed and discussed. All in all, the method used in this work has demonstrated to be well suited to account for the rich variety of experimental information available on the nuclear GT response. The global properties of the energy distributions of the GT strength and the $2\nu\beta\beta$ NMEs are reasonably well reproduced, the exception is the detailed description of the low-lying GT strength distributions that

could clearly be improved. It will be interesting in the future to extend these calculations by including all the double- β decay candidates and to explore systematically the potential of this method.

Acknowledgments

We are grateful to E. Moya de Guerra for useful discussions. This work was supported in part by MINECO

(Spain) under Research Grant No. FIS2011-23565 and by Consolider-Ingenio 2010 Programs CPAN CSD2007-00042.

-
- [1] J. Suhonen and O. Civitarese, Phys. Rep. **300**, 123 (1998); A. Faessler and F. Šimkovic, J. Phys. G: Nucl. Part. Phys. **24**, 2139 (1998); H. V. Klapdor-Kleingrothaus, *Seventy Years of Double Beta Decay*, World Scientific, Singapore (2010).
- [2] A. S. Barabash, Phys. Rev. C **81**, 035501 (2010).
- [3] Y. Fujita, B. Rubio, and W. Gelletly, Prog. Part. Nucl. Phys. **66**, 549 (2011).
- [4] D. Frekers, P. Puppe, J. H. Thies, and H. Ejiri, Nucl. Phys. A **916**, 219 (2013).
- [5] S. Rakers *et al.*, Phys. Rev. C **71**, 054313 (2005).
- [6] M. Sasano *et al.*, Phys. Rev. C **85**, 061301(R) (2012).
- [7] C. J. Guess *et al.*, Phys. Rev. C **83**, 064318 (2011).
- [8] P. Sarriguren, Phys. Rev. C **86**, 034335 (2012).
- [9] P. Sarriguren, O. Moreno, and E. Moya de Guerra, Rom. Journ. Phys. **58**, 1242 (2013).
- [10] C. Wrede *et al.*, Phys. Rev. C **87**, 031303(R) (2013).
- [11] P. Sarriguren, E. Moya de Guerra, A. Escuderos, and A. C. Carrizo, Nucl. Phys. A **635**, 55 (1998); P. Sarriguren, E. Moya de Guerra, and A. Escuderos, Nucl. Phys. A **658**, 13 (1999); Nucl. Phys. A **691**, 631 (2001).
- [12] P. Sarriguren, E. Moya de Guerra, and A. Escuderos, Phys. Rev. C **64**, 064306 (2001).
- [13] R. Álvarez-Rodríguez, P. Sarriguren, E. Moya de Guerra, L. Paceaescu, A. Faessler, and F. Šimkovic, Phys. Rev. C **70**, 064309 (2004).
- [14] D. Vautherin and D. M. Brink, Phys. Rev. C **5**, 626 (1972); D. Vautherin, Phys. Rev. C **7**, 296 (1973).
- [15] A. Chabanat, P. Bonche, P. Haensel, J. Meyer, and R. Schaeffer, Nucl. Phys. A **635**, 231 (1998).
- [16] M. Beiner, H. Flocard, N. Van Giai, and P. Quentin, Nucl. Phys. A **238**, 29 (1975).
- [17] N. Van Giai and H. Sagawa, Phys. Lett. B **106**, 379 (1981).
- [18] P. Moeller and J. Randrup, Nucl. Phys. A **514**, 1 (1990).
- [19] K. Muto, E. Bender, and H. V. Klapdor, Z. Phys. A **333**, 125 (1989); K. Muto, E. Bender, T. Oda, and H. V. Klapdor-Kleingrothaus, Z. Phys. A **341**, 407 (1992).
- [20] H. Homma, E. Bender, M. Hirsch, K. Muto, H. V. Klapdor-Kleingrothaus, and T. Oda, Phys. Rev. C **54**, 2972 (1996).
- [21] M. S. Yousef, V. Rodin, A. Faessler, and F. Šimkovic, Phys. Rev. C **79**, 014314 (2009).
- [22] D. Fang, A. Faessler, V. Rodin, M. S. Yousef, and F. Šimkovic, Phys. Rev. C **81**, 037303 (2010).
- [23] F. Šimkovic, L. Paceaescu, and A. Faessler, Nucl. Phys. A **733**, 321 (2004).
- [24] O. Moreno, R. Álvarez-Rodríguez, P. Sarriguren, E. Moya de Guerra, F. Šimkovic, and A. Faessler, J. Phys. G: Nucl. Part. Phys. **36**, 015106 (2009).
- [25] S. Singh, R. Chandra, P. K. Rath, P. K. Raina, and J. G. Hirsch, Eur. Phys. J. A **33**, 375 (2007).
- [26] D. L. Fang, A. Faessler, V. Rodin, and F. Šimkovic, Phys. Rev. C **82**, 051301(R) (2010).
- [27] M. T. Mustonen and J. Engel, Phys. Rev. C **87**, 064302 (2013).
- [28] J. Kotila and F. Iachello, Phys. Rev. C **85**, 034316 (2012).
- [29] I. Hamamoto and H. Sagawa, Phys. Rev. C **62**, 024319 (2000).
- [30] D. R. Bes, O. Civitarese, and J. Suhonen, Phys. Rev. C **86**, 024314 (2012).
- [31] O. Civitarese and J. Suhonen, Phys. Rev. C **89**, 044319 (2014).
- [32] J. Suhonen and O. Civitarese, Nucl. Phys. A **924**, 1 (2014).
- [33] F. Osterfeld, Rev. Mod. Phys. **64**, 491 (1992).
- [34] G. F. Bertsch and I. Hamamoto, Phys. Rev. C **26**, 1323 (1982).
- [35] E. Caurier, G. Martinez-Pinedo, F. Nowacki, A. Poves, and A. P. Zuker, Rev. Mod. Phys. **77**, 427 (2005).
- [36] J. Suhonen and O. Civitarese, Phys. Lett. B **725**, 153 (2013).
- [37] A. Faessler, G. L. Fogli, E. Lisi, V. Rodin, A. M. Rotunno, and F. Šimkovic, J. Phys. G: Nucl. Part. Phys. **35**, 075104 (2008).
- [38] J. Barea, J. Kotila, and F. Iachello, Phys. Rev. C **87**, 014315 (2013).
- [39] E. Caurier, F. Nowacki, and A. Poves, Phys. Lett. B **711**, 62 (2012).